Proceedings of the American Control Conference
Chicago, Illinois • June 2000

MODELLING A PNEUMATIC SERVO POSITIONING SYSTEM WITH FRICTION

Bashir M. Y. Nouri, Farid Al-Bender, Jan Swevers, Paul Vanherck and Hendrik Van Brussel.

Katholieke Universiteit Leuven
Mechanical Engineering Department , Div. of Production Eng., Machine Design and Automation
Celestijnenlaan 300 B, B-3001 Heverlee, Leuven, Belgium.
E-mail: Bashir.Nouri@mech.kuleuven.ac.be

Abstract: This paper treats the problem of modelling and identification of the various elements of a pneumatic servo positioning system to the end of constructing a complete and effective model that can be used for simulation and accurate control of such systems. Particular attention is paid to two important elements that manifest a strong nonlinear behaviour, viz. air flow and friction. In the first instance, an empirical model connecting the pneumatic valve's driving voltage, the pressures upstream and downstream, and the flow is hypothesised based on the nozzle formula. With this model, the flow function is then systematically identified. As regards friction, the Leuven model structure is used as basis for identification. Here, the two basic friction regimes, viz. pre-sliding, with its hysteresis behaviour, and gross sliding are well exposed and their essential parameters identified.

1. Introduction

The pneumatic cylinder is the most common actuator in industry. The traditional cylinder is a cheap and simple component compared with other electromechanical actuators of equal power density. However it is not competitive in applications where demands on accuracy, versatility and flexibility are important.

The main disadvantages of the pneumatic servo positioning systems are that, they are inherently nonlinear, that the compressibility of air results in very low stiffness (compared with the hydraulic system) leading to low natural frequency, and that low damping of the actuator system makes it difficult to control, especially with the presence of nonlinearities, time varying effects and position dependence. The pneumatic servo positioning system contains several nonlinearities such as the air flow-pressure relationship through the variable area orifice of the valve, the compressibility of air, and the (nonlinear) friction between the contacting surfaces of the slider-piston system. To overcome the disadvantages of a pneumatic servo positioning system and for the purpose of control and simulation, all the nonlinearities of the system must be modelled: this is the aim of this paper.

This paper is organised as follows: Section2 describes the used test set-up. Section 3 drives an empirical model of the flow through a variable area orifice of the 5-port proportional valve. Section 4 presents a theoretical model of the pneumatic rodless cylinder. Section 5 outlines the problem of friction modelling, demonstrating and identifying frictional behaviour in the two basic regimes of pre-sliding and gross sliding. Section 6 concludes the paper with some comments and statements.

2. Test Set-up

A schematic representation of the test apparatus is shown in Fig. 1. It consists of a 5-port proportional valve (FESTO, MPYE-5-1/8 HF-010B) and a rodless pneumatic cylinder (FESTO, DGPIL-25-1250-GK-KF-AH). Air flows from the (upstream) air tank (the supply) to the chambers of the cylinder is governed in magnitude and direction by the position of the valve's spool. The spool of the valve is actuated by an electromagnetic actuator (a solenoid). The electromechanical part of the servo valve is controlled by a feedback system that has a bandwidth of a bout 70 Hz so that, in this frequency range, the position of the spool is approximately proportional to the input signal.

The two differential pressure sensors are used for measuring the pressure difference between the chambers of the cylinder; which is proportional to the driving force. The position sensor is non-contacting eddy current sensor with a range of about 2 mm and is used for measuring the pre-sliding displacement. (The cylinder is equipped with an integrated ultrasonic position sensor that is, however, not used in these experiments owing to its limited resolution). The acceleration is measured by a carrier signal, inductive accelerometer, with frequency range of 0-250 Hz. The velocity is then obtained by integrating the acceleration. A computer is used for providing the driving input voltage to the valve by means of a D/A converter and reading the transducers by means of A/D converters.

3. Modelling the 5-Port Proportional Valve

This section derives an empirical model of the air flow through the variable area orifice of 5-port proportional valve, in function of the pressures at the supply point and at the pneumatic cylinder i.e. including the flow resistance of the connecting tubes and fittings, and the (quasi-static) valves driving voltage. The model is derived with the aid of the test set-up that is obtained by replacing the two sides of the pneumatic cylinder by two tanks of fixed known volumes.

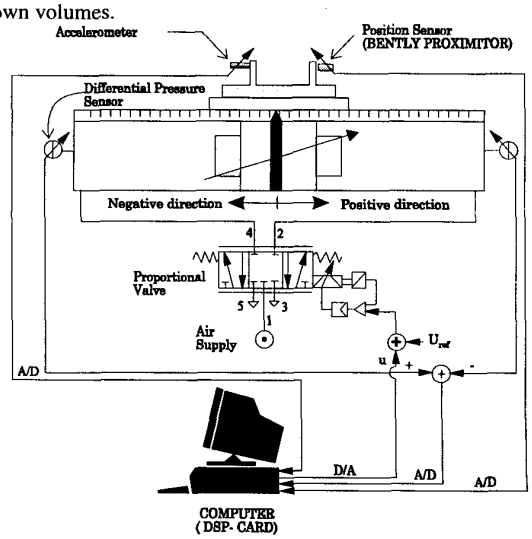

Fig. 1: Schematic diagram of the experimental set-up.

3.1 Model structure for the flow

The nozzle formula [3] is used as qualitative basis for our model. For a single orifice, the ideal isentropic mass flow rate is given by:

$$\dot{m} = A_{eff}\, P_1\, C(R,T_1,\kappa)\, \psi_T(P_2/P_1) \qquad (1)$$

with $$C(R,T_1,\kappa) = \sqrt{\frac{2\kappa}{RT_1(\kappa+1)}}\left[\frac{2}{\kappa+1}\right]^{1/(\kappa+1)} \qquad (2)$$

and

$$\psi_T = \begin{cases} \left(\frac{\kappa+1}{2}\right)^{\frac{1}{\kappa-1}} \sqrt{\frac{\kappa+1}{\kappa-1}\left[\left(\frac{P_2}{P_1}\right)^{\frac{2}{\kappa}} - \left(\frac{P_2}{P_1}\right)^{\frac{\kappa+1}{\kappa}}\right]}, & \bar{P}_{crit} \le \frac{P_2}{P_1} \le 1 \\ 1, & 0 < \frac{P_2}{P_1} \le \bar{P}_{crit} \end{cases} \qquad (3)$$

where: P_1 and P_2 are the absolute pressures upstream and down stream the orifice respectively, A_{eff} is the effective flow area of the orifice, $\bar{P}_{crit}$ is the critical pressure ratio ($\bar{P}_{crit} = 0.528 = b$), κ is the isentropic constant, R is gas constant, and T_1 is the absolute upstream temperature. In particular, the function ψ_T shows saturation behaviour for $P_2/P_1 < \bar{P}_{crit}$, corresponding to choked flow. It can easily be shown that the flow function for more than one orifice in series, taking P_1 and P_2 as the inlet and outlet pressures, will be different from that for a single orifice. In particular, $\bar{P}_{crit} \to b^n$, for n identical orifices. Moreover, the flow characteristic ψ could be direction dependent. If their be, in addition, other flow resistance elements in the pneumatic circuit (e.g. tubes, bends, etc.), it would be rather pointless to try to fit the experimental data with the ideal nozzle formula. On the other hand, it would be reasonable to expect that an empirical model would have the same structure as that of a series (of an unknown number) of arbitrary orifices; i.e. the flow parameters and their combinations will remain basically unaltered. Our task boils down then to identifying $A_{eff} \times \psi(P_2/P_1)$ where $0 \le \psi \le 1$ while retaining $P_1 \times C(R, T, \kappa)$. Further, if, for a given A_{eff} (which is proportional to the driving voltage lul), ψ will saturate for a sufficiently small P_2/P_1, as is often the case in practice, it will then be possible and expedient to distinguish between the two terms A_{eff} and ψ, which would otherwise be lumped together.

3.2 Valve Flow Equation

A systematic series of experiments have been performed to determine the flow rate through the orifices of the proportional valve as a function of the valve's driving signal, downstream and upstream pressures. In these experiments, the valve is first set at its neutral position (U_{ref} = 5 volt). Then, for a given spool DC voltage, u, and supply pressure, P_S (or initial tank pressure respectively), the pressure variation in the tank, that is being charged or discharged, is measured in real time. For simplicity and since only an empirical model is sought for, the process is assumed isothermal throughout ($T = T_{ref} = T_{atm}$ e.g.). Hence, we have PV = mRT, where V, R and T are constants (V = volume of a tank, P = absolute pressure in the tank, m = mass of air in the tank). Differentiating and rearranging yields:

$$\dot{m} = \frac{V}{RT}\dot{P} \qquad (4)$$

That is to say that the mass flow rate can be obtained by differentiating the tank-pressure measurements in the time. In practice, however, since direct differentiation of the (noisy) experimental data can be quite cumbersome, a more creative identification procedure has been used as will be sketched in the following. First of all, the valve effective area A_{eff}, as a function of the valve driving voltage and the upstream pressure, can be identified, up to a constant factor, as follows. Since, for a given constant upstream pressure, the downstream pressure satisfies $\dot{P} \sim A_{eff}\, \psi(P)$, then, separating the variables P and t and integrating yields

$$F(P) = \int \frac{dP}{\psi(P)} \sim \int A_{eff}\, dt = A_{eff}\, t \qquad (5)$$

This function, F, represents the tank pressure evolution that is measured in the experiment, see Fig. 2-a. The result means that, for a fixed upstream pressure, the downstream pressure evolution should have the same form when the time axis is scaled by a factor proportional to the effective area, see Fig. 2-b. Thus, for a group of tank pressure evolution curves corresponding to the same upstream pressure, a best fit of those curves is sought onto one another using the scaling factors as fitting parameters. In this way (i) the dependence of the effective area on the valve driving voltage is determined and (ii) a single best fit is sought for the whole group, which is then used to identify ψ. Summing up, the mass flow rate through the valve is modelled by the formula

$$\dot{m} = (\pm) A_{eff} P_1 \sqrt{\frac{2\kappa}{RT(\kappa+1)}}\left[\frac{2}{\kappa+1}\right]^{1/(\kappa+1)} \psi(P_2/P_1) \qquad (6)$$

where: $\pm$ indicates the direction of the flow. ψ and A_{eff} are to be experimentally identified.

As regards the effective orifice area of the valve, the identification results show that it is primarily a function of the driving voltage and, to a lesser extent, the supply pressure as shown in Fig. 3.

$$A_{eff} = A_m \frac{\left(1 - \left(\frac{u - U_S}{U_o - U_S}\right)^C\right)^D}{a_2 P_S^2 + a_1 P_S + a_o} \qquad (7)$$

where, A_m is the maximum achievable effective area, u, U_S, and U_o are the proportional valve's driving, saturation and dead zone voltages respectively, C, D, a_o, a_1, and a_2 are constants and P_S is the absolute supply pressure.

As for the function ψ, two qualitatively similar, but quantitatively different forms were identified; namely corresponding to charging and discharging respectively. The difference arises not only from the direction dependence of the flow, that has been

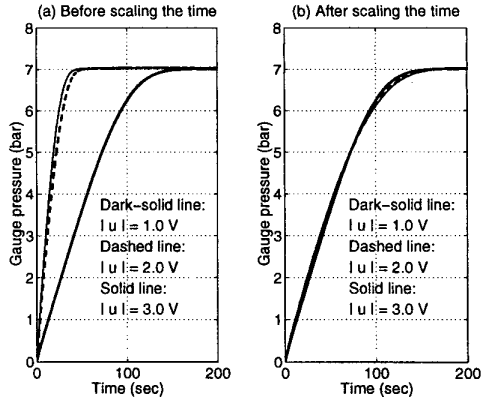

Fig. 2: Measured pressures in a downstream tank; charging through orifice 1,4. Supply pressure = 7 bar (gauge).

alluded to earlier, but also from the fact that, for discharging, an extra flow resistance element has been added at the outlet; viz. a silencer to subdue exhaust noise. These two functions are given by:

Charging: $$\psi_C = \left(1 - \left[(P_2/P_S - b)/(1-b)\right]^{\beta}\right)^{\gamma} \quad (8)$$

Discharging: $$\psi_D = \sum_{n=0}^{n=12} A_n \left(\frac{P_{atm}}{P_2}\right)^n \quad (9)$$

where: β, γ and A_n are constants, and the parameter b is the critical (saturation) pressure ratio. Identification shows that b = -0.6682. Negative critical pressure ratio means that the flow never saturates (or "chokes"). Fig. 4 plots the theoretical air flow factor, for a single ideal nozzle, ψ_T, together with those experimentally identified for charging, ψ_C and the discharging, ψ_D.

4. Theoretical Model of the Rodless Pneumatic Cylinder

4.1 Flow into the cylinder vs. piston displacement

Fig. 5 shows a schematic diagram of the cylinder. Two control volumes may be identified, one control volume (V_i) on either side of the piston. Each control volume consists of a variable active volume (V_{iA}) and a constant dead volume (V_{iD}). Applying the ideal gas equation of state to the two control volumes and assuming isothermal process as before, i.e. $T_1 = T_2 = T$, yields:

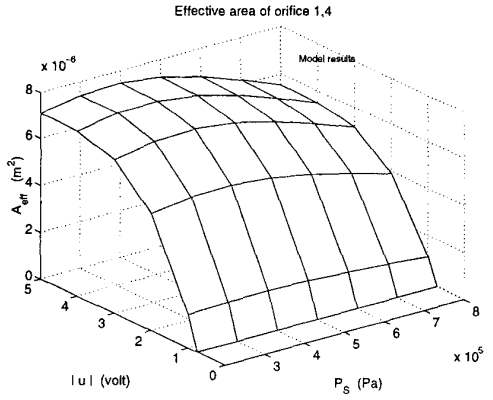

Fig. 3: A_{eff} of orifice 1,4; model results.

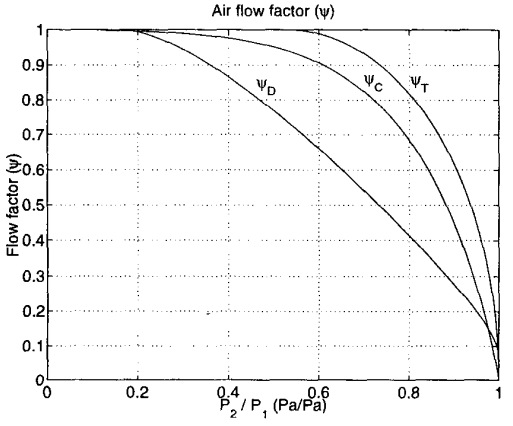

Fig. 4: Comparison between ψ_T, ψ_C and ψ_D air flow factors.

$$P_1(Ax + V_{1D}) = m_1 RT \quad (10)$$

$$P_2(A(L-x) + V_{2D}) = m_2 RT \quad (11)$$

where A is the cross-sectional area of the piston.

Differentiating the above equations yields the sought for dynamic equations, namely:

$$\dot{P}_1 = \frac{RT}{Ax + V_{1D}}\dot{m}_1 - \frac{AP_1}{Ax + V_{1D}}\dot{x} \quad (12)$$

$$\dot{P}_2 = \frac{RT}{A(L-x)+V_{2D}}\dot{m}_2 + \frac{AP_2}{A(L-x)+V_{2D}}\dot{x} \quad (13)$$

4.2 Piston and payload

The piston and payload (slider mass) are modelled by using Newton's second law; i.e. the total applied force (F) on the piston is equal to the inertia force of the sliding body plus the friction force (F_f).

$$F = M\ddot{x} + F_f \quad (14)$$

where M is the total sliding mass that is composed of the piston's mass, the mass of the sliding table and the mass of an object (work piece) rigidly coupled to the sliding table. The total applied force (F) is equivalent to the chambers' differential pressure times the cross sectional area (A) of the pneumatic cylinder. Equation 15 gives the acceleration of the slide body.

$$\ddot{x} = \frac{A}{M}(P_1 - P_2) - \frac{1}{M}F_f \quad (15)$$

Up to this point, all the basic elements of the system have been identified and modelled except the friction force, which will be dealt with hereunder.

5. Modelling the Friction Force

Friction is perhaps the most important nonlinearity that is found in any mechanical system with moving parts. For the system considered in this paper, friction, which arises in the contacts of the piston with the cylinder walls as well as in the linear slide-way and other minor rubbing elements, has a direct impact on the dynamics of the system in all regimes of operation. In order accurately to design compensation, friction has to be identified and modelled. This task is by no means a simple one since no universal friction model exists, on the one hand, and the practical measurement of friction is not straightforward, on the other. A good model structure for the identification of friction would ease the aforementioned task.

5.1 Model structure

The most comprehensive friction model structure to be found in the open literature is perhaps the described in [5] and [7], the so- called Leuven model. It represents refinement and generalisation on an earlier model proposed by [2] especially in regard to the friction hysteresis in the "pre-sliding" regime, which has particular relevance to our case. Consequently, the above mentioned model

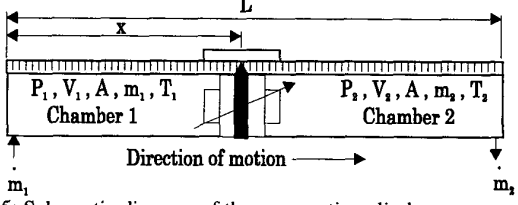

Fig. 5: Schematic diagram of the pneumatic cylinder.

structure has been adopted in the present investigation on friction in our system. With this model structure, the friction force, F_f, is modelled (globally) by a set of two equations that depend on a state variable, z, representing the average deformation of asperities on the contacting surfaces, on its time derivative and on the sliding velocity, v. Thus:

$$F_f = F_h(z) + \sigma_1 \frac{dz}{dt} + \sigma_2 v \qquad (16)$$

where σ_1 is micro-viscous damping coefficient that is usually negligibly small and σ_2 is the viscous damping coefficient. $F_h(z)$ is the hysteresis friction force that is modelled by a hysteresis function consisting of transition curves (curves between two reversal points or extrema). Each velocity reversal initiates a new transition curve, adds a new extremum to the hysteresis memory, and resets the state variable z to zero. The transition curve which is active at a certain time will be called the current transition curve, and is represented by $F_d(z)$, which is a point-symmetric strictly increasing function of z. The value of $F_h(z)$ at the beginning of a transition curve is represented by F_b, hence:

$$F_h(z) = F_b + F_d(z) \qquad (17)$$

Finally, the nonlinear state equation is based on the current hysteresis transition curve and the current velocity:

$$\frac{dz}{dt} = v\left(1 - \mathrm{sgn}\left(\frac{F_d(z)}{S(v) - F_b}\right) * \left|\frac{F_d(z)}{S(v) - F_b}\right|^n\right) \qquad (18)$$

where, S(v) models the constant velocity behaviour in the sliding (the Stribeck effect, see later) and the exponent n allows to model the difference between dz/dt and v especially at the transition from pre-sliding to sliding. In view of the above, our task becomes basically that of identifying $F_d(z)$, S(v), n, σ_1 and σ_2; the first two and the last one being the most important.

5.2 Pre-sliding friction identification

The aim here is to measure the friction force in function of the displacement, prior to gross sliding, and to verify its hysteretic behaviour. Fig. 6 shows a typical friction hysteresis loop measurement corresponding to cylinder pressure variation around a 7 bar level. The point-symmetry of the loop can be verified by plotting the inverted lower half and the upper half on top of one other. It is clear from Fig. 6 that the force tends to saturate with increasing displacement. As a matter of fact, just after saturation, gross sliding will suddenly ensue. The value of the saturation force corresponds to the value of what is usually termed "static friction" or "break-away force", F_S. The displacement corresponding to the start of gross slip is termed the pre-sliding distance x_h. It can be seen that, for our system, this value is ~0.25 mm. Since the desired positioning accuracy will fall well below this value, this pre-sliding hysteresis behaviour, which practically has no dynamics, see e.g. [4], will play an important role in designing the control system. Further , for the purpose of implementation in the controls, this pre-sliding hysteresis curve can be approximated by a continuous smooth or piece-wise linear function on the interval $0 \le x < x_h$. This function may then be used to determine the function $F_d(z)$ using the relations (16 through 18).

There are two main types of hysteretic behaviour. Firstly, hysteresis with *nonlocal* memory means that the future values of the function (friction force in this case) at some instant of time t, ($t \ge t_0$) depend not only on its present value at the instant of time t_0 and the value of its argument (displacement in this case) but also on the past extremum values of the function. This property is in contrast to the behaviour of hysteresis nonlinearities with *local* memory, where the past has its influence upon the future through the current value of the function) [6]. The *nonlocal* memory character of pre-sliding hysteresis friction, in our system, has been thoroughly verified by test. For this purpose, a periodic piston motion trajectory is chosen with several velocity reversal points (per period), within the pre-sliding region, and the friction force and position have been recorded. When these two sets of synchronised data are plotted against each other, an external loop is obtained with several internal loops within it (Fig. 7).

5.3 Implementation of the hysteresis model

The implementation of the hysteresis model in programming requires the provision of two memory stacks: one for the minima of F_h in ascending order (stack min), and one for the maxima of F_h (stack max). The stacks grow at a velocity reversal and shrink when an internal hysteresis loop is closed. When the system goes from pre-sliding to sliding, the stacks are reset. The value of the state variable z is reset to zero at each velocity reversal and recalculated at the closing of an internal loop, see [5] and [7].

5.4 Friction at gross sliding: Velocity dependence

We now turn our attention to the identification of the function S(v) and the coefficient σ_2 in the adopted model structure, i.e. the velocity dependence aspect. This is usually expressed in the form of Stribeck curve, which plots the friction force in function of the steady state speed. In order to obtain this sort of data, however, the slide has to be run at a constant speed while the friction force is recorded, for a large number of speeds in the range of interest.

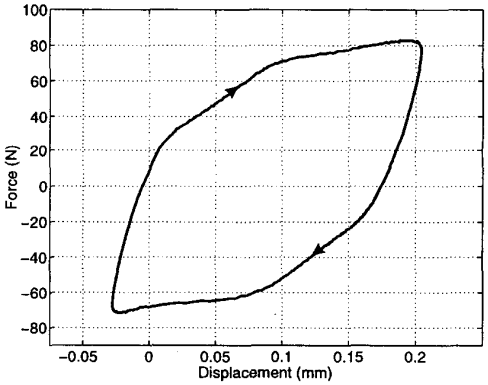

Fig. 6: Typical measured hysteresis friction loop.

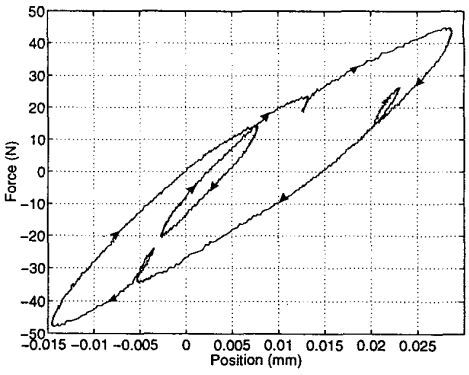

Fig. 7: Measured pre-sliding hysteresis with *nonlocal* memory.

Such a procedure is however almost impossible to execute on our system when it is pneumatically actuated since it will require perfect control of the speed for which this investigation is a pre-requisite. Instead, the line followed in this study is to excite the system so as to move periodically in the desired speed range, approximately $|v| \leq 2$ m/s, while recording the friction force. A series of tests have been carried out on the test set-up (Fig. 1). Typical results obtained with this procedure are depicted in Fig. 8, which plots the friction force in function of the velocity at different nominal chamber pressures corresponding to supply pressures of 2 through 7 bar (gauge), with steps of 1 bar. The results, which proved to be very repeatable, show quite clearly the hysteretic behaviour of friction in the velocity or what is termed "frictional lag" (w. r. t. velocity change), see e.g. [1]. That is to say that the friction force is higher for increasing speed (and lower for decreasing speed) than the quasi-static Stribeck value.

The Stribeck behaviour is very well in evidence, for the increasing speed part of the loop, this behaviour is usually modelled as follows:

$$F_f = S(v) + \sigma_2 v \tag{19}$$

where, $$S(v) = F_C + \left(F_S - F_C\right)e^{-(v/v_s)^{\delta}} \tag{20}$$

where F_C is the Coulomb friction, F_S the static friction, v_s the Stribeck velocity and δ an arbitrary exponent. For decreasing speed, however, the behaviour seems very consistently to resemble that of Coulomb plus viscous friction.

In order to use these results for modelling we can either (i) make a best fit of the Stribeck model parameters (i.e. F_C, F_S etc.), insert these values in the integrated friction model structure (equations 16-18) and subsequently tune the remaining parameters (especially the exponent n in Equation 18) so that the resulting model correspond as best as possible to the experimental data, or (ii) fit the data separately for each branch of the hysteresis loop shown in Fig. 8 and implement the results directly in the controls design. The latter method will lead to a discontinuous model involving many switches that is cumbersome to implement. On the other hand, it may suffice to follow the first line of action leading to a more grossly estimated behaviour, but that is much easier to implement.

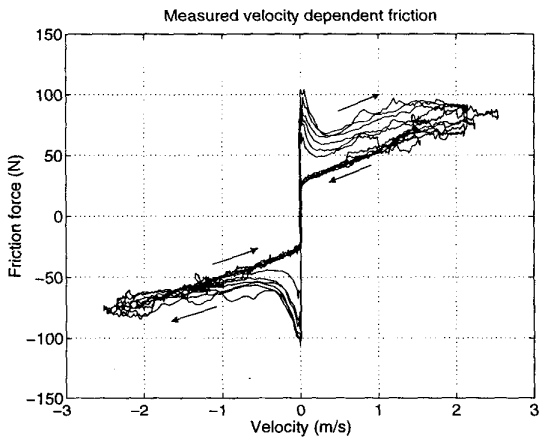

Fig. 8: Measured velocity dependent friction force in the positive and negative directions, and for different supply pressures.

6. Conclusion

The most essential elements of a pneumatic servo positioning system have been identified/modelled effectively. These elements are all characterised by a strong nonlinear behaviour, so that identification is strongly connected to the choice of an appropriate model structure. First, the servo valve's driving voltage-pressure-flow relation is identified and modelled based on the single nozzle model structure. Although the latter proved sufficient for modelling/identification purpose, the form of the flow-pressure function actually obtained significantly departs from the nozzle formula that is commonly used for modelling servo valves. Moreover, two different functions have been obtained for charging to the cylinder and for discharging to atmosphere, respectively, such might be important for accurate control design. Creative identification procedures have been devised to validate the models and quantify their parameters. Second, the friction characteristics of the sliding components (piston and carriage) have been carefully identified. Based on the most advanced integrated friction model structure, the frictional characteristics during pre-sliding as well as during gross sliding have been successfully determined. In particular, the nonlocal memory character of frictional hysteresis in pre-sliding has been well demonstrated.

Further work will proceed in three steps, vis. (i) constructing an overall simulation model for the pneumatic servo system in order to establish conformity of behaviour with practice and gain some idea about general behaviour, (ii) design effective controls and validate them on the simulation model, and (iii) implement the most promising of the latter controls on the existing system, which is the underlying goal of the research presented in this paper.

Acknowledgement

This text presents research results of the Belgian programme on Interuniversity Poles of attraction initiated by the Belgian State, Prime Minister's Office, Science Policy Programming. The scientific responsibility is assumed by its authors.

References

[1] Armstrong-Hélouvry, B. (1991), "Control of Machines with Friction," Kluwer Academic Publishers, London.

[2] Canudas de Wit, C., H. Olsson, K. Aström, and P. Lischinsky, (1995), " A new model for control of systems with friction," IEEE Transactions on Automatic Control, 40(5): 419-425.

[3] Fox, Robert W., and McDonald, Alan T, (1994), "Introduction to fluid mechanics," Fourth Edition, John Willey & Sones, INC.

[4] Futami, S., Furutani, A., and Yoshida, S. (1990), "Nanometer positioning and its micro-dynamics," Nanotechnology, No.1, pp 31-37.

[5] Ganseman, C., J. Swevers, T. Prajogo, and F. Al-Bender (1997), "An integrated friction model with improved presiding behaviour," In IFAC Symposium on Robot Control, Nantes, France, pp. 159-164.

[6] Mayergoyz I. D. (1991), "Mathematical Models of Hysteresis," Springer-Verlag New York Inc.

[7] Swevers, J., F. Al-Bender, C. Ganseman, and T. Prajogo (1999), "An integrated friction model structure with improved presliding behaviour for accurate friction compensation," Accepted for puplication in IEEE Trans. On Automatic Control.